IEEE Access
Multidisciplinary | Rapid Review | Open Access Journal

Received July 10, 2021, accepted July 25, 2021, date of publication July 28, 2021, date of current version August 10, 2021.

Digital Object Identifier 10.1109/ACCESS.2021.3100933

A Compact Dual-Band and Dual-Polarized Millimeter-Wave Beam Scanning Antenna Array for 5G Mobile Terminals

YUQI HE[1], (Student Member, IEEE), SIHAN LV[1], LUYU ZHAO[1], (Senior Member, IEEE), GUAN-LONG HUANG[2], (Senior Member, IEEE), XIAOMING CHEN[3], (Senior Member, IEEE), AND WEI LIN[4], (Senior Member, IEEE)

[1]Key Laboratory of Antennas and Microwave Technologies, Xidian University, Xi'an 710071, China
[2]School of AI-Guangdong & Taiwan, Foshan University, Foshan, Guangdong 528225, China
[3]School of Information and Communications Engineering, Xi'an Jiaotong University, Xi'an 710049, China
[4]Global Big Data Technologies Centre, The University of Technology Sydney, Ultimo, NSW 2007, Australia

Corresponding author: Luyu Zhao (lyzhao@xidian.edu.cn)

This work was supported in part by the National Key Research and Development Program of China under Grant 2019YFF0216603, in part by the Key Research and Development Program of Shaanxi under Grant 2020ZDLGY15-03, in part by ZTE Corporation under Grant HC-CN-20191227012, in part by the Natural Science Foundation of China under Grant 61801300, and in part by the Fok Ying-Tong Education Foundation, China, under Grant 171056.

ABSTRACT This paper presents a compact dual-band and dual-polarized millimeter-wave patch antenna array with satisfactory performance on element mutual coupling and beam scanning capabilities. Using capacitive feed technique and stacked configuration with extra parasitic strips, the proposed antenna array is able to achieve a wide operating bandwidth in both the low- and high-bands. In order to reduce the array's footprint, and to enhance the beam scanning performance in both bands, the element spacing is shrunk to less than 0.36 wavelength at 26 GHz. To improve the isolation between array elements due to their small spacings, two effective decoupling approaches are adopted, which result in a 6-dB isolation enhancement. The overall size of the proposed antenna array is only 18.2 mm $\times$ 4.1 mm $\times$ 1.07 mm, which is smaller than some industrial mm-Wave antenna modules released recently. Our simulation shows that the antenna array can fully cover the 5G NR bands of n258$\sim$n261 simultaneously. The four-element array provides $\pm 60^\circ$ and $\pm 45^\circ$ beam scanning performance in the low- and high-bands, respectively. The experimental data of reflection coefficient, mutual coupling, and radiation patterns confirm with the simulated results, rendering the proposed array to be a good candidate for 5G mm-Wave communications.

INDEX TERMS 5G, dual-band, dual-polarization, mm-Wave, mobile phone antennas, microstrip antenna, phased array.

I. INTRODUCTION

Millimeter-wave (mm-wave) technologies for 5G applications attract more and more attentions after the 2019 World Radiocommunication Conference (WRC-19), where a series of globally unified resolutions on mm-Wave frequency bands for International Mobile Telecommunications (IMT) are accomplished. As shown in Fig. 1, currently, the major 5G mm-Wave bands licensed worldwide include 24.25-27.5 GHz, 37-43.5 GHz, 45.5-47 GHz, 47.2-48.2 GHz, and 66-71 GHz [1]. Therefore, these newly-released frequency bands bring additional design specifications and challenges for mm-Wave antennas compared with conventional Sub-6 GHz antennas, especially in the mobile terminal scenario [2]. To overcome the relatively high path-loss in the mm-Wave band and to increase the beam coverage capability, phased arrays with wide scanning angles are a preferred solution in mm-Wave antenna designs for mobile phone applications [3]–[6]. Meanwhile, the mainstream antenna arrays tend to cover as much 5G NR (New Radio) bands (cf. Table 1) as possible. Hence, dual-band/multi-band designs of antenna array become a necessity. On the other hand, to enable multiple-input multiple-output (MIMO) operations and alleviate the multipath fading effect, a dual-polarized antenna

The associate editor coordinating the review of this manuscript and approving it for publication was Wei Feng.

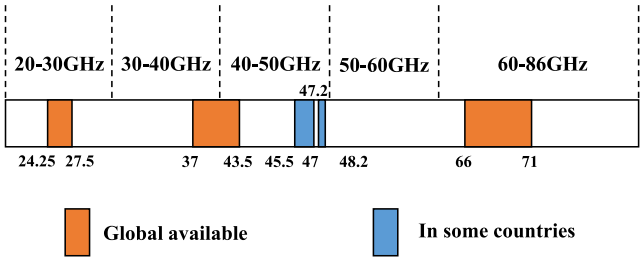

FIGURE 1. IMT mm-Wave bands allocated by WRC-19.

TABLE 1. Specifications of 5G mm-Wave Bands.

NR Operating Band	Uplink and Downlink Frequency Range	Duplex Mode
n257	26.50 GHz-29.50 GHz	TDD
n258	24.25 GHz-27.50 GHz	TDD
n259	39.50 GHz-43.50 GHz	TDD
n260	37.00 GHz-40.00 GHz	TDD
n261	27.50 GHz-28.35 GHz	TDD

TDD: Time Division Duplex; NR: New Radio.

array is also demanded. Consequently, the mm-Wave antennas in mobile phone are expected to offer multi-band coverage with dual-polarized function, meanwhile they must be constructed in a limited size to form a compact antenna module. Such design specifications are very challenging for not only the academia but also the industry.

At present, there are already many innovative antenna designs proposed for mm-Wave mobile termial applications. In [7], a broadband coverage of 27-29 GHz is achieved by three well designed slot arrays. In [8], the proposed beam controllable collinear dipole array can operate from 22 GHz to 34 GHz. In [9], a mm-Wave magneto-electric monopole antenna with vertically polarized end fire radiation is presented, which achieves both low profile and broadband coverage of 23.5-44 GHz characteristics. In [10], a multi-beam antenna array with differential feed is proposed with an operating bandwidth of 26.8-29.2 GHz. In [11], hybrid mode technique is used to improve the bandwidth of the cavity backed mm-Wave slot antenna. In [12], a 5G mm-Wave phased array antenna configured with novel end-fire planar folded slot antennas (PFSA) is proposed to operate at 37-39 GHz. The above-mentioned designs all demonstrate effecvtive array solutions in mm-Wave band. However, they only operate in single band, which cannot comply with the IMT regulations that at least two bands have to be covered. In [13], a design scheme of mm-Wave broadband coverage using capacitance-feed and simple structure is proposed, which covers a broadband of 24-28 GHz in the form of single polarization. In [14], a dual-band and single-polarized antenna array operating at 28/38 GHz bands is obtained by utilizing novel photonics-based reconfigurable strategy. Nevertheless, to mitigate the multipath fading and to enable the MIMO operation for higher data rates, the antenna array in a mobile terminal is preferable to generate two orthogonal polarizations [15]–[18]. Furthermore, for a phased array integrated in a limited volume of a mobile terminal, it is still necessary to reduce the communcation blind zone and achieve wide-angle beam steering [19]. As presented in [20], a compact patch antenna array operating in the band of 26-31.4 GHz is able to provide $\pm 42^\circ$ beam coverage via beam switching. A dual-polarized mm-Wave antenna array operating in the band of 24.4-29.5 GHz with a scanning angle from -34° to 33° was proposed in [21]. Though these designs achieve certain promising performance, the scanning angle still needs to be extended in practical applications. The antennas proposed in [13] and [22] perform good performance with more than $\pm 60^\circ$ beam scanning angle, yet they all occupy a large volume and are infeasiable for mobile phones as the mainstream mm-Wave antenna modules are installed in the side frames which are only several centimeters wide. From another aspect, the spacing between the neighboring antenna elements in the array must be less than 0.5 λ so as to avoid grating lobes at large scanning angles. However, too close spacing will inevitably lead to strong coupling between antenna elements. Though many decoupling methods have been reported in recent years [23]–[25], their application scenarios in mm-Wave terminals are limited.

Apart from the academic research, industries also provide some competitive antenna solutions. The latest mm-Wave module QTM052 from Qualcomm® covers a bandwidth of 800 MHz including Bands n258, n260 and n261 [26] with a size of 19.03 mm $\times$ 4.81 $\times$ 1.7 mm^3. It is reported that the mm-Wave module of Apple's newly released iPhone 12 can cover Bands n260 and n261 with dual-polarization [27]. According to the public information, the module adopts the design strategy of separating low- and high-band antennas, which results in a relatively large module size.

This paper mainly discusses an effective solution to meet the above-mentioned requirements and proposes a compact dual-band and dual-polarized patch antenna array with decoupling structures, which operates in the frequency bands of 26 GHz and 38 GHz. A 4-element antenna array based on this solution is able to provide $\pm 60^\circ$ and $\pm 45^\circ$ beam scanning capability in the two frequency bands, respectively. Compared to the existing mm-Wave antenna array designs, the design presented in this paper has the follow unique features:

1) Dual-Polarized characteristic with multiband coverage is enabled by advanced feeding design and elaborate parasitic structures.
2) The array is very compact in size due to the innovative decoupling approach utilized in the low-band.
3) A better beam scanning capability is achieved and experimentally verified for practical application, especially for the low-band.

The remaining part of this paper is organized as follows: Section II introduces the design of the dual-band antenna element; Section III illustrates the antenna array design with a focus on the decoupling technique; Section IV presents

the fabrication details of the antenna prototype as well as its performance evaluation; Conclusion will be drawn in Section V.

II. DESIGN OF ANTENNA ELEMENT

In this section, a dual-band and dual-polarized antenna element is designed in the 5G NR bands. The low-band (LB) and high-band (HB) cover 24.25-28.35 GHz and 37-43.5 GHz, respectively. The structural configuration of the proposed antenna element is shown in Fig. 2. It is a stacked patch structure, where the bottom large patch (Fig. 2(b)) is used to generate a lower resonant frequency while the smaller patch on the top (Fig. 2(c)) is for higher resonant frequency. Dual-probe feeding method is utilized to achieve ±45° linear polarizations. As is well-known, the probe-feed method would introduce additional inductive effect to the antenna [28]. Therefore, to increase the operating frequency band, power is coupled from the two probes to the bottom patch through two circular plates, which are realized by cutting two ring slots on the bottom patch. Compared with directly connecting to the patch, such indirect feeding brings additional capacitance to counteract the inductiveness from the probe-feed. Moreover, four corners of the bottom square patch are cut-off to further fine tune its resonant frequency and reduce the footprint of the patch. The upper patch works at 39 GHz band. Better impedance matching and higher gain are achieved by opening a square aperture in the middle of the patch. Additionally, four bent parasitic strips are introduced around the upper patch to generate an extra resonant mode near the 41 GHz band so as to broaden the operating bandwidth in the HB.

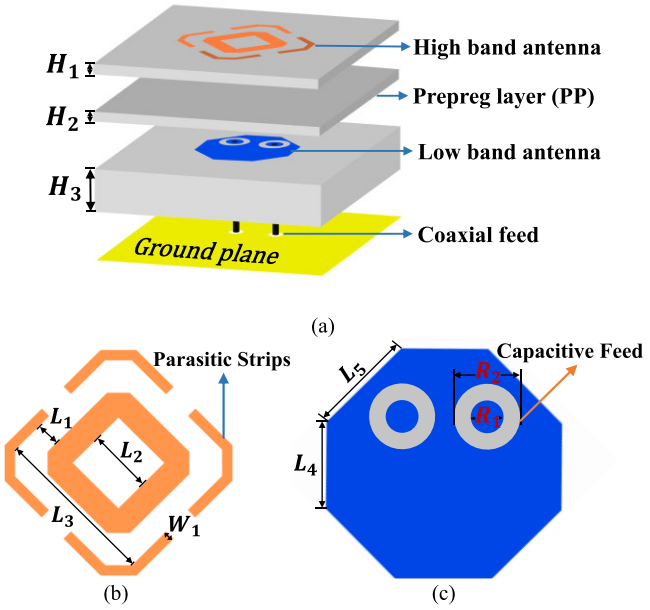

FIGURE 2. Geometrical configuration of the proposed mm-Wave antenna element. (a) 3D view. (b) Sketch of the HB patch. (c) Sketch of the LB patch.

TABLE 2. Detailed Dimensions of the Proposed Antenna (unit: mm).

Variable	Value	Variable	Value	Variable	Value
H_1	0.205	L_1	0.36	L_8	1.85
H_2	0.1	L_2	0.92	L_9	0.75
H_3	0.762	L_3	1.67	L_{10}	30.6
H_4	0.1	L_4	0.88	W_1	0.15
H_5	0.205	L_5	1.02	W_2	0.2
R_1	0.21	L_6	1.21	W_3	18.0
R_2	0.37	L_7	0.7	/	/

The antenna element is implemented by using the printed circuit board (PCB) technology. Rogers RO4350B (εr= 3.52) is used for the double-layer dielectric substrate, and Rogers RO4450F with a thickness of 4 mils is functioned as a prepreg (pp) layer which is utilized to bond different layers together. Detailed dimensions of the antenna element are list in Table 2. The antenna element is modeled by Ansys HFSS®, and its scattering parameters (S-parameters) in both LB and HB are superposed in Fig. 3. The results indicate a better than −10 dB reflection coefficient (represented by $|S_{11}|$) over the frequency bands of 24.2-27.7 GHz and 36.2-43.8 GHz is achieved, which can fully cover the required 5G NR mm-Wave frequency bands. In addition, Fig. 3 shows the reflection coefficient performance of the element without capacitance-feeding structure, from the comparison of which it can be seen that the operating bandwidth of the antenna is greatly increased from 1.6 GHz to 3.5 GHz in the LB. Also, the S-parameters of the HB element with and without the parasitic structures and the opening square aperture are shown in Fig. 3, from which one can observe that these structures greatly improve the impedance matching and port isolation in the HB. Fig. 4 and Fig. 5 shows the current distributions of different structures of the antenna element at different operating frequencies when the port 1 and 2 is excited. Fig. 4 (a) and Fig. 5 (a) are the current distribution of the LB antenna at 26 GHz, Fig. 4 (b) and Fig. 5 (b) show the current distribution of the HB antenna at 38 GHz, while Fig. 4 (c) and Fig. 5 (c) display the current distribution of the parasitic strips at 41 GHz.

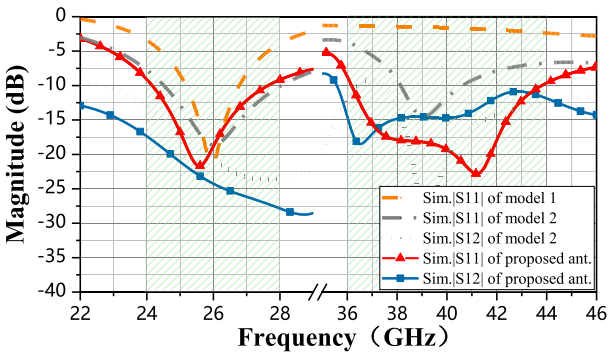

Model 1: without capacitive feed structure
Model 2: without parasitic structures and square aperture
Proposed ant. : with capacitive feed structure, parasitic structures and square aperture

FIGURE 3. Simulated S-parameters of the antenna element at two operating bands.

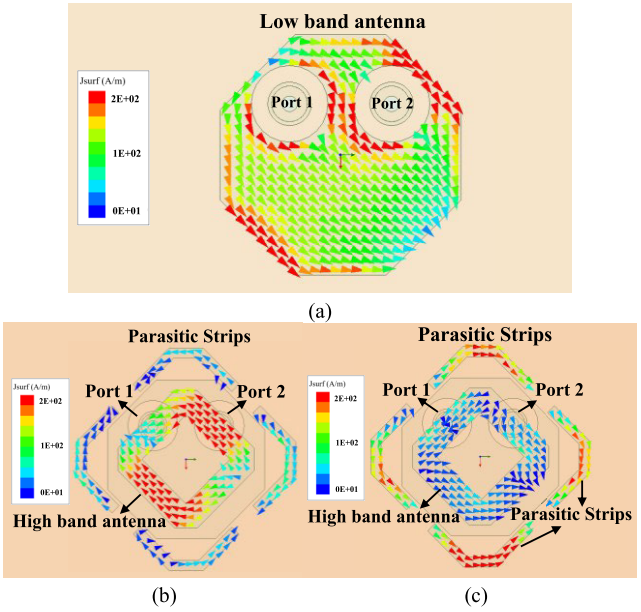

FIGURE 4. Current distribution of different structure of antenna element when the port 1 is excited. (a) Low band antenna at 26 GHz. (b) High band antenna at 38 GHz. (c) Parasitic strips at 41 GHz.

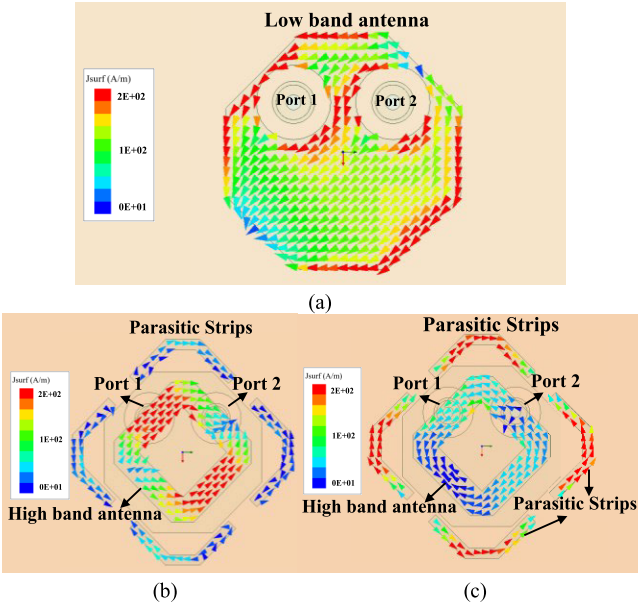

FIGURE 5. Current distribution of different structure of antenna element when the port 2 is excited. (a) Low band antenna at 26 GHz. (b) High band antenna at 38GHz. (c) Parasitic strips at 41 GHz.

Fig. 6 shows the simulated far-field radiation patterns of the antenna element. The maximum gain value is found to be 5.8 dBi at 28 GHz and 6.2 dBi at 39 GHz, with at least 20 dB XPD (cross-polarization discrimination) at 26 GHz and 15 dB XPD at 39 GHz. The half-power beamwidth (HPBW) of the antenna element are 112° at 26 GHz and 98° at 39 GHz. The radiation pattern of the back lobe is larger at HB, which is caused by the larger size of the high-frequency parasitic strips structure relative to the ground plane.

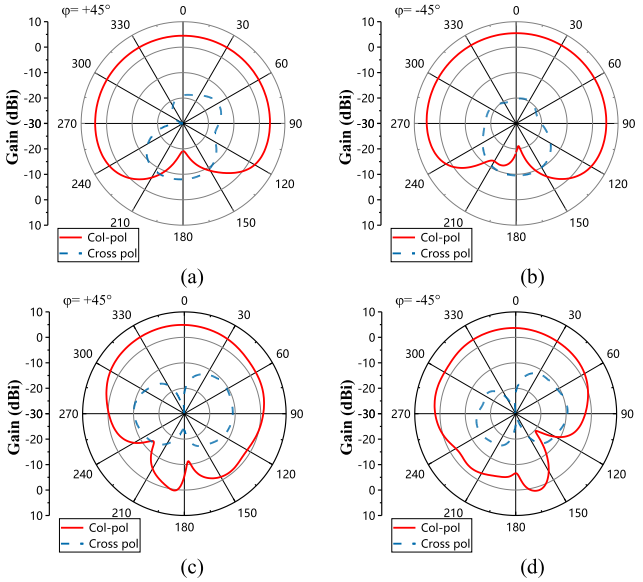

FIGURE 6. Simulated radiation patterns of the two orthogonal polarizations (pol.) of the antenna elements at LB and HB. (a) +45° pol. at 26 GHz. (b) −45° pol. at 26 GHz. (c) +45° pol. at 39 GHz. (d) −45° pol. at 39 GHz.

III. DESIGN OF THE ANTENNA ARRAY

A. CONSIDERATION OF MODERATE AND COMPACT ELEMENT ARRANGEMENTS

In 5G mobile terminals, very limited space is reserved for mm-Wave phased arrays because of the existence of the Sub-6 GHz antennas, as well as the metal frames and full display screen. Both the miniaturized design of the antenna unit as discussed in the previous section and the reduced spacing of antenna elements will effectively contribute to a size reduction of the mm-Wave antenna array. However, for a dual-band antenna array, there is always a dilemma between the element spacing and array performance. For instance, once the physical distance between the array elements is around $\lambda/2$ at 26 GHz in the LB, the size of the array will be relatively large in the HB, and grating lobes will be generated during beam scanning since the element spacing in the HB is now greater than 0.75λ at 39 GHz. Such situation is called moderate arrangement in this work. In contrast, if the element spacing is chosen to be about $\lambda/2$ at 39 GHz, the mutual coupling in the LB will significantly increase as the corresponding spacing in the LB is only 0.36λ at 26 GHz. This case is called compact arrangement. Therefore, according to the above analysis, the moderate arrangement of array elements will lead to large grating lobes in the HB while the compact arrangement will result in strong mutual coupling in the LB, which inevitably affects the antenna radiation efficiency and causes scanning blindness. In order to balance the array size and performance, the compact arrangement is chosen while effective decoupling approaches are taken in this work to deal with the resulting mutual coupling in the LB.

As shown in Fig. 7, the array is formed by four dual-band antenna elements with an element spacing of 4.2 mm

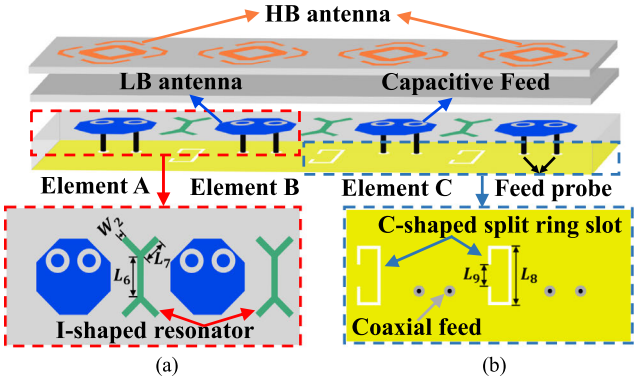

FIGURE 7. 4-element patch antenna array with decoupling structures. (a) I-shaped resonator. (b) C-shaped split ring slot.

(equivalent to 0.36 λ at 26 GHz and 0.5 λ at 39 GHz). The overall dimension of the antenna array is 18.2 mm × 4.1 mm × 1.07 mm. Two sets of decoupling structures are adopted, i.e., the modified I-shaped parasitic resonators between the elements (see Fig. 7(a)) and the C-shaped split ring slot (SRS) etched on the ground plane (see Fig. 7(b)).

B. DECOUPLING STRUCTURE DESIGN

In order to clearly demonstrate the effectiveness of the two proposed structures on mutual coupling suppression between the antenna elements, the current distributions of the two elements in the proposed antenna array with respect to different configurations are given in Fig. 8, respectively.

As shown in Fig. 8 (a), when Port 2 is excited, it is observed that a direct and strong coupling (S_1) appears between Element A and Element B. To start with, the coupling between the two antenna elements can be effectively reduced by etching the C-shaped split ring slot etched on the ground plane, as shown in Fig. 8 (b), at this time the coupling between antenna Elements A and B is reduced to S_2.

Besides the C-shaped SRSs, I-shaped parasitic resonators are also introduced between the LB antenna elements to further improve their isolations, as shown in Fig. 8 (c), the typical electrical length of the parasitic I-shaped resonators is around half wavelengths at the center frequency of the LB. In addition, both ends of the I-shaped parasitic resonator are bent to minimize its electrical length, providing a capacitive load to control the magnitude of coupling between the adjacent antenna elements. While in Fig. 8 (c), a new coupling route (S_3) can be artificially generated through the I-shaped parasitic resonator. By changing the width (W_2) and lengths (L_6 & L_7) of the I-shaped parasitic resonator, the amplitude and phase of the coupling introduced by the I-resonator can be adjusted properly so as to cancel out the existing coupling S_1, the remaining coupling is marked as S_3 in Fig. 8 (c).

In addition, when two different decoupling structures are added separately, the induced currents in antenna Element B are in opposite directions (S_2 and S_3), which allows the currents to cancel each other when two decoupling structures

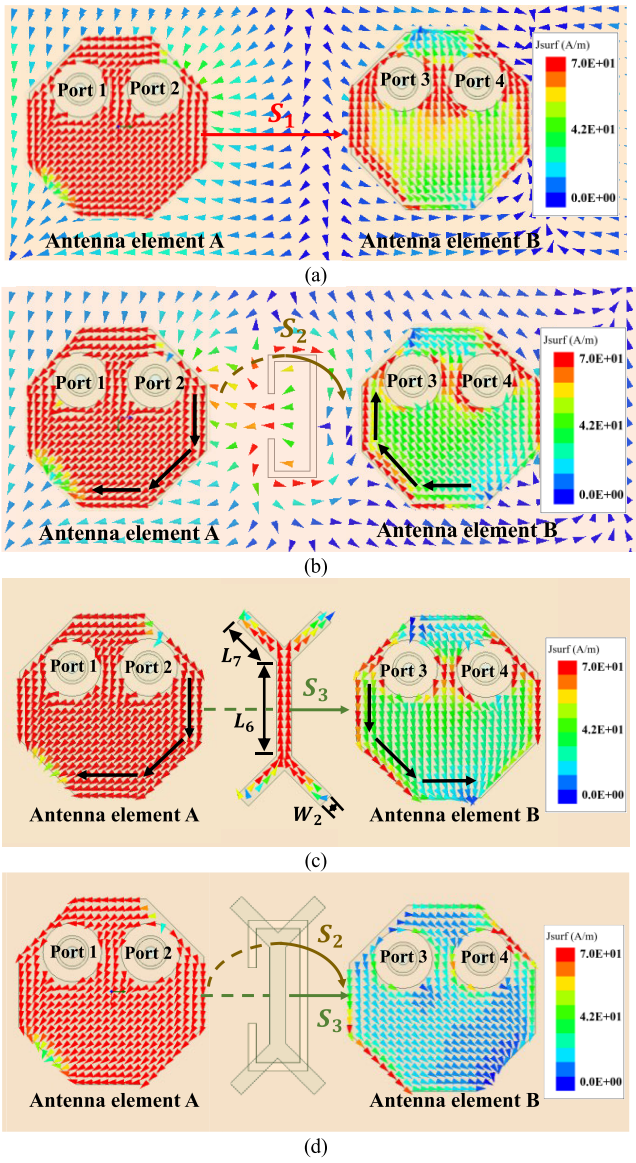

FIGURE 8. Vector current distribution of the two elements in the proposed antenna array. (a) Without the I-shaped resonator and the C-shaped SRSs. (b) With the C-shaped SRSs only. (c) With the I-shaped resonator only. (d) With the I-shaped resonator and the C-shaped SRSs.

are added simultaneously. Eventually, the proposed antenna array with two decoupling structures could further reduce the coupling to a much lower level as shown in Fig.8 (d).

As can be seen from the EM simulation results shown in Fig. 9, after introducing the I-shaped resonator between the antenna elements and the C-shaped SRS etched on the ground plane, the cross-polarization (x-pol.) isolation levels can be improved by around 6 dB. Fig. 10 shows the co-polarization (co-pol.) isolation in the array. In addition, the co-polarization isolation between antenna elements is increased by 11 dB at most. It is worth mentioning that the two decoupling methods have no impact on antenna matching performance, and it will be shown in the next session that isolations among all elements in the array are better than 15 dB, demonstrating that

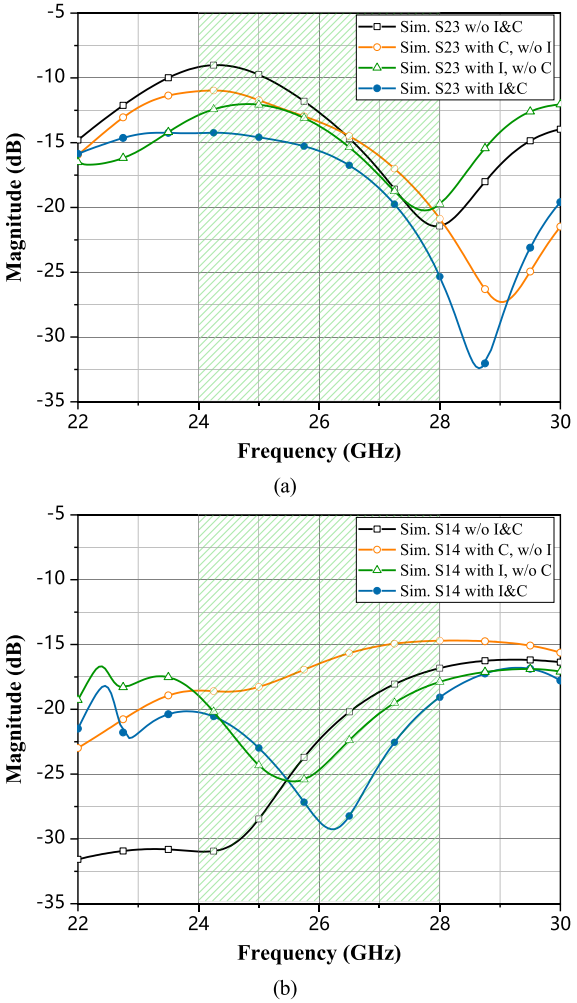

FIGURE 9. Impact of the decoupling approaches on the cross-polarization isolation improvement between the antenna elements. (a) Isolation between Port 2 and Port 3. (b) Isolation between Port 1 and Port 4.

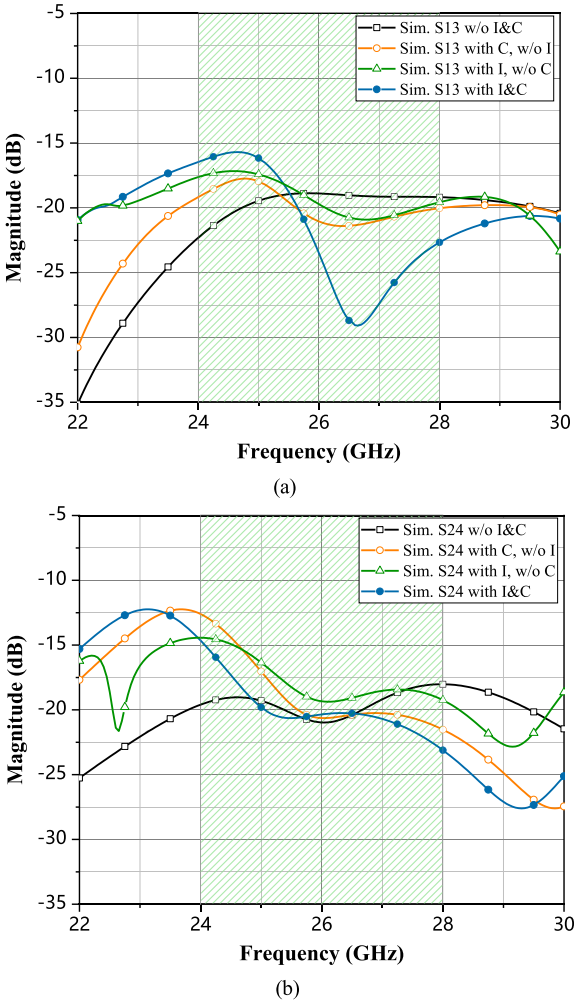

FIGURE 10. Impact of the decoupling approaches on the co-polarization isolation improvement between the antenna elements. (a) Isolation between Port 1 and Port 3. (b) Isolation between Port 2 and Port 4.

they are effective decoupling techniques for the mm-Wave application.

IV. PERFORMANCE EVALUATION AND DISCUSSION

In order to validate the simulated results, a prototype of the proposed array antenna is fabricated and measured. It should be noted that the size of the mini-SMP (SMPM) connectors used in the mm-Wave measurement is comparable to the antenna itself. Therefore, for successful installment of the connectors, the ground plane is expanded to be 30 mm $\times$ 185 mm. An explosive-view and the layout of the bottom layer of the proposed antenna array are demonstrated in Fig. 11 and Fig. 12, respectively. As can be seen from Fig. 12, the footprints of the SMPM connectors will affect the integrity of the ground plane 2. Therefore, to ensure that the antenna array has a complete reflection ground plane, a two-layer grounding structure is constructed, which are connected by metallized vias as shown in Fig. 11. In these layers, the ground plane 1 is used to prevent the

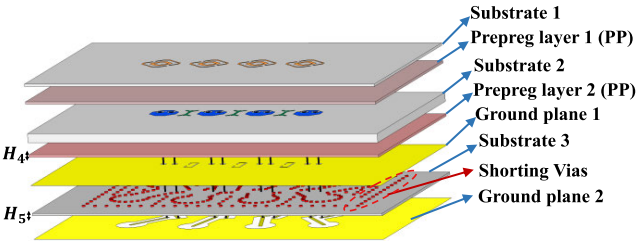

FIGURE 11. Structure and layer stack of the proposed 4-element antenna array.

joint package affecting the antenna performance. In ground plane 1, eight metallized vias are constructed for signal transmitting from the SMPM connectors to the LB antenna elements. In addition, 301 metallized shorting vias are drilled between grounding layers 1 and 2 to maintain excellent electrical contact. All the dielectric substrates 1, 2 and 3 are Rogers 4350B. Detailed dimensions of the antenna array are list in Table 3.

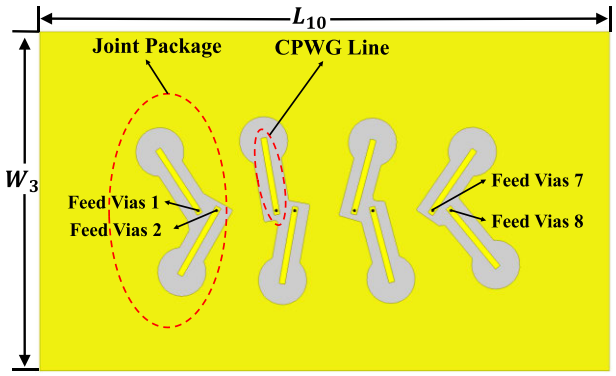

FIGURE 12. Layout of the bottom layer of the array prototype.

TABLE 3. Detailed Dimensions of the Antenna Array (unit: mm).

Variable	Value	Variable	Value	Variable	Value
H_4	0.1	L_7	0.7	L_{10}	30.6
H_5	0.205	L_8	1.85	W_2	0.2
L_6	1.21	L_9	0.75	W_3	18.0

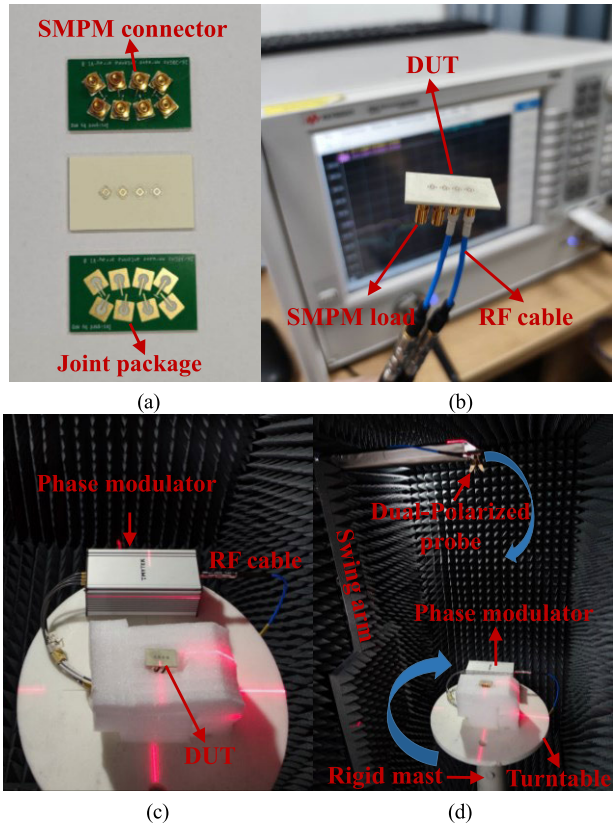

FIGURE 13. Prototype and measurement setup. (a) Prototype of the proposed 4-element antenna array. (b) Measurement setup of S-parameters. (c) Array under test with a phase modulator (BBox). (d) Measurement setup of radiation patterns.

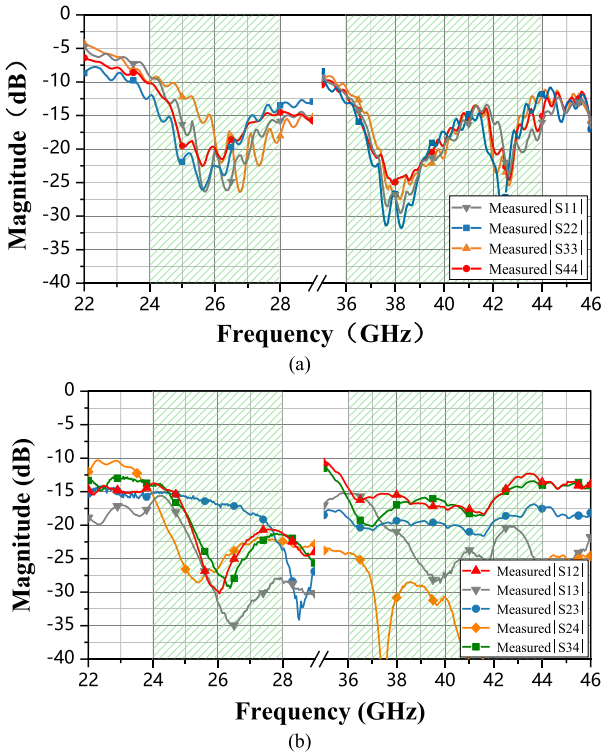

FIGURE 14. Measured S-parameters of the proposed antenna. (a) Reflection coefficient. (b) Isolation.

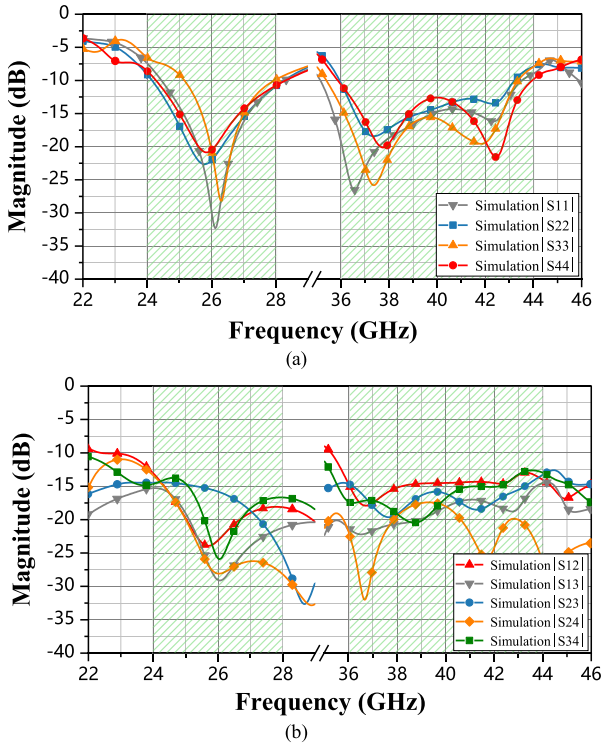

FIGURE 15. Simulated S-parameters of the proposed antenna. (a) Reflection coefficient. (b) Isolation.

According to the array stacked figure shown in Fig. 11, an array prototype is fabricated and measured, as shown in Fig. 13. The antenna array is measured by a two-port Keysight N5225A network analyzer. During the measurement, when the two orthogonal ports of one antenna element are under test, the other six ports are terminated with 50 Ω

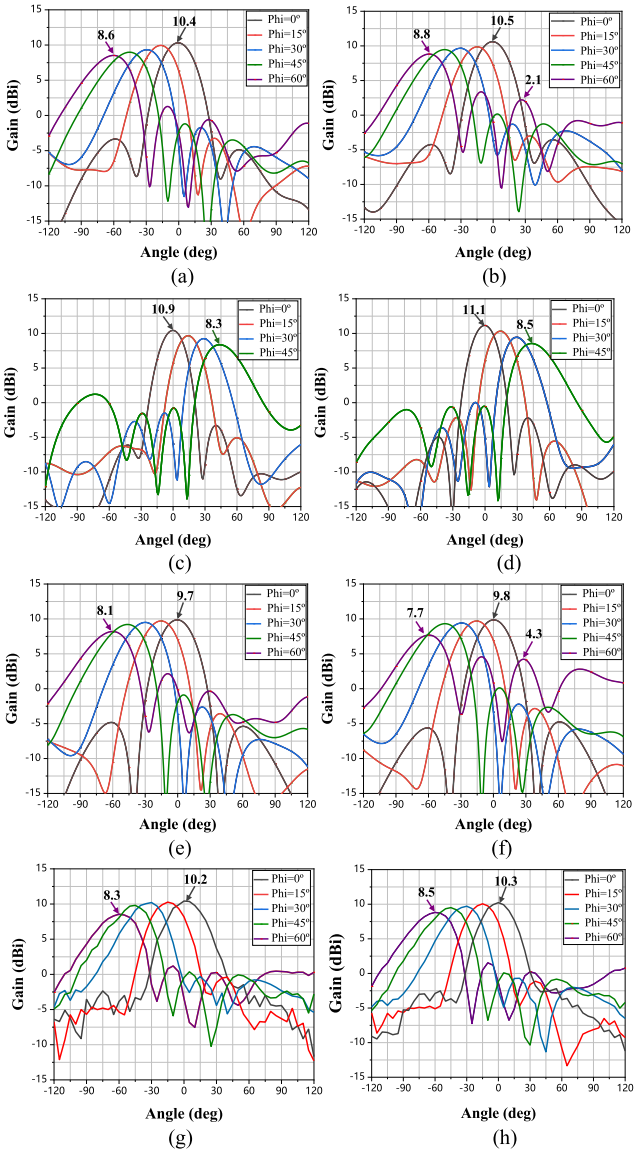

FIGURE 16. 2D beam scanning patterns of the antenna array in the plane of theta = 90°. (a) Simulated patterns of +45° polarization at 26.6 GHz for proposed antenna array. (b) Simulated patterns of −45° polarization at 26.6 GHz proposed antenna array. (c) Simulated patterns of +45° polarization at 38 GHz proposed antenna array. (d) Simulated patterns of −45° polarization at 38 GHz proposed antenna array. (e) Simulated patterns of +45° polarization at 26.6 GHz for antenna array without decoupling structure. (f) Simulated patterns of −45° polarization at 26.6 GHz for antenna array without decoupling structure. (g) Measured patterns of +45° polarization at 26.6 GHz. (h) Measured patterns of −45° polarization at 26.6 GHz.

SMPM loads, as shown in Fig. 12(b). The measured and simulated S-parameters are shown in Fig. 14 and Fig. 15, respectively, which are in good agreement with each other. The passive experimental results validate that the antenna array can well cover the bands of 24-28 GHz and 36-42 GHz simultaneously with all port isolations better than 15 dB.

As mentioned previously, beam scanning capability is a key figure of merit for mm-Wave antenna arrays in a 5G mobile terminal. Therefore, the beam scanning angle of the

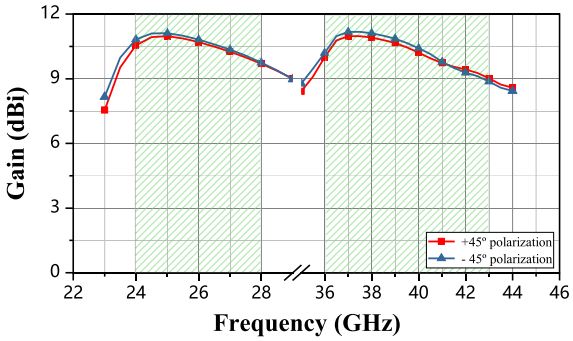

FIGURE 17. Simulated realized gain with respect to the +45° polarization and −45° polarization of the antenna array.

proposed array is evaluated by both simulation and measurement. As shown in Figs. 16(a) and (b), the EM simulation shows that the scanning angle of the proposed antenna array can reach ±63° at 26.6 GHz, and the scanning angle is about ±45° at 38 GHz as plotted in Figs. 16(c) and (d). In addition, the simulation patterns of the antenna array without decoupling structures are given in Figs. 16(e) and (f). It can be seen that both the scanning angle and the gain of the proposed antenna array are improved, and the sidelobe levels of the radiation patterns are also reduced. The beam scanning ability of the antenna array is also measured with the help of TMYTEK® phase modulator, BBOX One [29], at 26 GHz to verify the consistency between the simulation and actual measurement.

The antenna pattern measurement environment is already shown in Fig. 13(c). Figs. 16(g) and (h) display the measured beam scanning diagrams of the antenna array at 26.6 GHz, which shows less than 0.2 dB gain discrepancy compared to the simulated ones. It should be noted that due to the symmetrical arrangement of the antenna array, the beam scanning performances of the two polarizations are basically the same. Also, the beam steering characteristics of the array for plus/minus (+/−) scanning angles are basically symmetric. Therefore, for simplification, only the beam scanning results of one direction are given in Fig. 16. Simulated realized gains shown in Fig. 17 are found to be around 10 dBi over the two band.

For a more visualized perception of the beam scanning capability, the proposed antenna array is placed on the short edge of a rectangular metallic board whose size mimics the actual size of a 5G flagship mobile phone. Fig. 18 and Fig. 19 show the three-dimensional beam scanning patterns of the 4-element antenna array in free space operating in different bands.

Furthermore, to emphasize the strength of the proposed mm-Wave antenna array, a comparison between the proposed design and several mm-Wave arrays reported recently is shown in Table 4. Some key antenna characteristics including operating band, antenna size, polarization diversity and beam scanning range are highlighted. After the comparison, it is clear that the proposed design not only achieves a

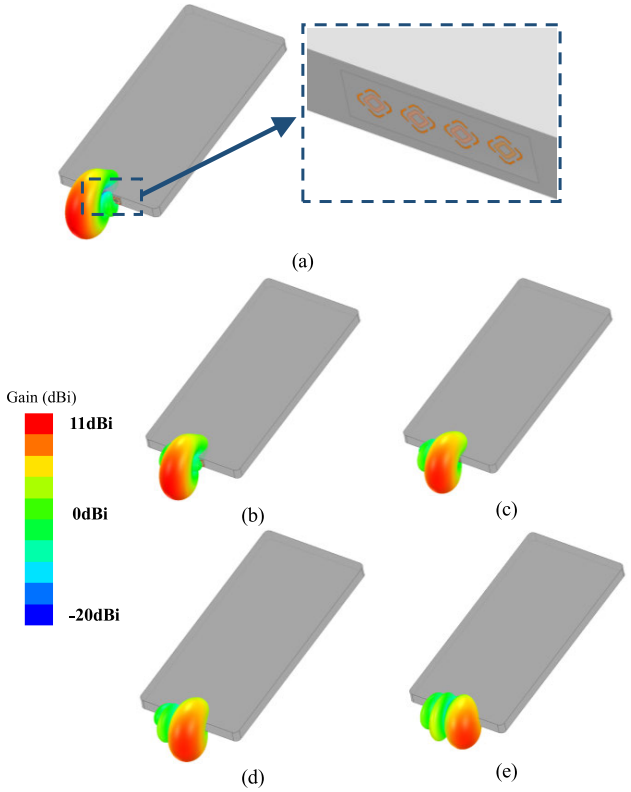

FIGURE 18. 3D beam scanning patterns of +45° polarization at 26 GHz with different phi angles in the plane of theta = 90°. (a) 0°. (b) 15°. (c) 30°. (d) 45°. (e) 60°.

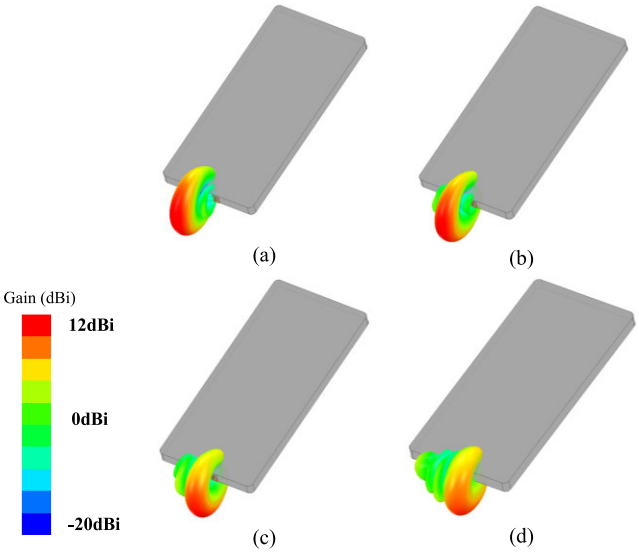

FIGURE 19. 3D beam scanning patterns of +45° polarization at 38 GHz with different phi angles in the plane of theta = 90°. (a) 0°. (b) 15°. (c) 30°. (d) 45°.

larger bandwidth in dual-band operation, but also provides a larger scanning angle in the two orthogonal polarizations, which can be a promising candidate for 5G mm-Wave mobile terminals.

TABLE 4. Comparison between the Proposed Design and Other Reported Works.

Ref.	Freq. (GHz)	BW (LB/LB) (GHz)	Ant. Size (mm)	Pol.	Beam Scanning (LB/HB)
[12]	37-39	2	15.6×1.8×0.89	Single linear	±50°
[13]	24-28	4	47.1×8.0×0.8	Single linear	±60°
[14]	27.6-30.8 36.8-38.4	3.2/1.6	48.9×1.0×3.56	Single linear	/
[16]	28-33	5	20.0×3.50×5.3	Dual linear	±40°
[22]	21-22	1	110×55.0×0.7	Single linear	±75°
Prop.	24-28 36-42	4/6	18.2×4.1×1.07	Dual linear	± 60° / ± 45°

Ref.: Reference; Freq.: Frequency; BW: Bandwidth; Ant.: Antenna; Pol.: Polarization; Prop.: Proposed.

V. CONCLUSION

In this paper, a dual-band and dual-polarized mm-Wave antenna array with decoupling structures has been proposed for 5G mobile terminal applications. The proposed design starts with the investigation of the antenna element, followed by two decoupling approaches for mutual coupling reduction in the low-band, the operating principle of which has also been analyzed in detail. Subsequently, the antenna array performances have been confirmed with the experimental results, which show that the isolation levels among all the eight ports are more than 15 dB in both the 24-28 GHz and 36-42 GHz bands, with reflection coefficients less than −10 dB. The beam scanning angles of the antenna array are about ±60° and ±45° in the LB and the HB, respectively. The satisfactory performance reveals the proposed antenna array can be a promising candidate for 5G mm-Wave mobile terminals.

ACKNOWLEDGMENT

The authors would like to express our gratitude to Xi'an Lambda Communication Technology Company Ltd., for providing the mm-Wave single probe near/far field mobile antenna measurement system, and TMY Technology Inc., for the help on the phase modulator BBOX. They would also like to thank Prof. Long Zhang and Prof. Sai-Wai Wong for preparation of the samples and helpful discussions.

REFERENCES

[1] *World Radiocommunication Conference 2019 (WRC-19), Final Acts*. Accessed: Nov. 2019. [Online]. Available: https://www.itu.int/pub/R-ACT-WRC.14-2019
[2] W. Hong, K.-H. Baek, and S. Ko, "Millimeter-wave 5G antennas for smartphones: Overview and experimental demonstration," *IEEE Trans. Antennas Propag.*, vol. 65, no. 12, pp. 6250–6261, Dec. 2017.
[3] B. Xu, K. Zhao, Z. Ying, D. Sjöberg, W. He, and S. He, "Analysis of impacts of expected RF EMF exposure restrictions on peak EIRP of 5G user equipment at 28 GHz and 39 GHz bands," *IEEE Access*, vol. 7, pp. 20996–21005, 2019.

[4] W. Hong, K.-H. Baek, Y. Lee, Y. Kim, and S.-T. Ko, "Study and prototyping of practically large-scale mmWave antenna systems for 5G cellular devices," *IEEE Commun. Mag.*, vol. 52, no. 9, pp. 63–69, Sep. 2014.

[5] J. Helander, K. Zhao, Z. Ying, and D. Sjöberg, "Performance analysis of millimeter-wave phased array antennas in cellular handsets," *IEEE Antennas Wireless Propag. Lett.*, vol. 15, pp. 504–507, Mar. 2016.

[6] J. Helander, D. Sjöberg, M. Gustafsson, K. Zhao, and Z. Ying, "Characterization of millimeter wave phased array antennas in mobile terminal for 5G mobile system," in *Proc. IEEE Int. Symp. Antennas Propag. USNC/URSI Nat. Radio Sci. Meeting*, Vancouver, BC, Canada, Jul. 2015, pp. 7–8.

[7] S. Zhang, X. Chen, I. Syrytsin, and G. F. Pedersen, "A planar switchable 3-D-coverage phased array antenna and its user effects for 28-GHz mobile terminal applications," *IEEE Trans. Antennas Propag.*, vol. 65, no. 12, pp. 6413–6421, Dec. 2017.

[8] D. Psychoudakis, Z. Wang, and F. Aryanfar, "Dipole array for mm-wave mobile applications," in *Proc. IEEE Antennas Propag. Soc. Int. Symp. (APSURSI)*, Orlando, FL, USA, Jul. 2013, pp. 660–661.

[9] J. Wang, Y. Li, J. Wang, L. Ge, M. Chen, Z. Zhang, and Z. Li, "A low-profile vertically polarized magneto-electric monopole antenna with a 60% bandwidth for millimeter-wave applications," *IEEE Trans. Antennas Propag.*, vol. 69, no. 1, pp. 3–13, Jan. 2021.

[10] Q. Yang, S. Gao, Q. Luo, L. Wen, Y.-L. Ban, X. Ren, J. Wu, X. Yang, and Y. Liu, "Millimeter-wave dual-polarized differentially fed 2-D multibeam patch antenna array," *IEEE Trans. Antennas Propag.*, vol. 68, no. 10, pp. 7007–7016, Oct. 2020.

[11] H. Li, Y. Cheng, L. Mei, and F. Wu, "Dual-polarized frame-integrated slot arrays for 5G mobile handsets," *IEEE Antennas Wireless Propag. Lett.*, vol. 19, no. 11, pp. 1953–1957, Nov. 2020.

[12] J. Park, H. Seong, Y. N. Whang, and W. Hong, "Energy-efficient 5G phased arrays incorporating vertically polarized endfire planar folded slot antenna for mmWave mobile terminals," *IEEE Trans. Antennas Propag.*, vol. 68, no. 1, pp. 230–241, Jan. 2020.

[13] M. Stanley, Y. Huang, H. Wang, H. Zhou, A. Alieldin, and S. Joseph, "A capacitive coupled patch antenna array with high gain and wide coverage for 5G smartphone applications," *IEEE Access*, vol. 6, pp. 41942–41954, 2018.

[14] I. F. da Costa, S. A. Cerqueira, D. H. Spadoti, L. G. da Silva, J. A. J. Ribeiro, and S. E. Barbin, "Optically controlled reconfigurable antenna array for mm-wave applications," *IEEE Antennas Wireless Propag. Lett.*, vol. 16, pp. 2142–2145, 2017.

[15] Y. He, M. Rao, Y. Liu, G. Jing, M. Xi, and L. Zhao, "28/39-GHz dual-band dual-polarized millimeter wave stacked patch antenna array for 5G applications," in *Proc. Int. Workshop Antenna Technol. (iWAT)*, Bucharest, Romania, Feb. 2020, pp. 1–4.

[16] R. M. Moreno, J. Ala-Laurinaho, A. Khripkov, J. Ilvonen, and V. Viikari, "Dual-polarized mm-wave endfire antenna for mobile devices," *IEEE Trans. Antennas Propag.*, vol. 68, no. 8, pp. 5924–5934, Aug. 2020.

[17] W. Hong, S.-T. Ko, Y. Lee, and K.-H. Baek, "Multi-polarized antenna array configuration for mmWave 5G mobile terminals," in *Proc. Int. Workshop Antenna Technol. (iWAT)*, Seoul, South Korea, Mar. 2015, pp. 60–61.

[18] R. M. Moreno, J. Kurvinen, J. Ala-Laurinaho, A. Khripkov, J. Ilvonen, J. van Wonterghem, and V. Viikari, "Dual-polarized mm-wave endfire chain-slot antenna for mobile devices," *IEEE Trans. Antennas Propag.*, vol. 69, no. 1, pp. 25–34, Jan. 2021.

[19] W. Hong, Z. H. Jiang, C. Yu, J. Zhou, P. Chen, Z. Yu, H. Zhang, B. Yang, X. Pang, M. Jiang, and Y. Cheng, "Multibeam antenna technologies for 5G wireless communications," *IEEE Trans. Antennas Propag.*, vol. 65, no. 12, pp. 6231–6249, Dec. 2017.

[20] K. Klionovski, M. S. Sharawi, and A. Shamim, "A dual-polarization-switched beam patch antenna array for millimeter-wave applications," *IEEE Trans. Antennas Propag.*, vol. 67, no. 5, pp. 3510–3515, May 2019.

[21] H. Li, Y. Li, L. Chang, W. Sun, X. Qin, and H. Wang, "A wideband dual-polarized endfire antenna array with overlapped apertures and small clearance for 5G millimeter-wave applications," *IEEE Trans. Antennas Propag.*, vol. 69, no. 2, pp. 815–824, Feb. 2021.

[22] N. Ojaroudiparchin, M. Shen, S. Zhang, and G. F. Pedersen, "A switchable 3-D-coverage-phased array antenna package for 5G mobile terminals," *IEEE Antennas Wireless Propag. Lett.*, vol. 15, pp. 1747–1750, 2016.

[23] F. Liu, J. Guo, L. Zhao, G.-L. Huang, Y. Li, and Y. Yin, "Dual-band metasurface-based decoupling method for two closely packed dual-band antennas," *IEEE Trans. Antennas Propag.*, vol. 68, no. 1, pp. 552–557, Jan. 2020.

[24] X. Shen, Y. Liu, L. Zhao, G.-L. Huang, X. Shi, and Q. Huang, "A miniaturized microstrip antenna array at 5G millimeter-wave band," *IEEE Antennas Wireless Propag. Lett.*, vol. 18, no. 8, pp. 1671–1675, Aug. 2019.

[25] J.-N. Hwang and S.-J. Chung, "Isolation enhancement between two packed antennas with coupling element," *IEEE Antennas Wireless Propag. Lett.*, vol. 10, pp. 1263–1266, 2011.

[26] *Qualcomm QTM052 mm-Wave Antenna Modules*. Accessed: Jul. 2018. [Online]. Available: http://www.qualcomm.com/products/qtm052-mmwave-antenna-modules

[27] *Apple's Mobile Phone-iPhone 12*. Accessed: Oct. 2020. [Online]. Available: http://www.apple.com/iphone-12/specs/

[28] H. Wong, K.-L. Lau, and K.-M. Luk, "Design of dual-polarized L-probe patch antenna arrays with high isolation," *IEEE Trans. Antennas Propag.*, vol. 52, no. 1, pp. 45–52, Jan. 2004.

[29] *TMYTEK Phase Modulator-BBOX One*. Accessed: Mar. 2020. [Online]. Available: http://www.tmytek.com/bbox

YUQI HE (Student Member, IEEE) received the B.S. degree from Xidian University, Xi'an, China, in 2019, where he is currently pursuing the M.D. degree in electromagnetic wave and microwave technology. His research interests include millimeter wave array, phased antenna array, and metamaterial-based antenna arrays.

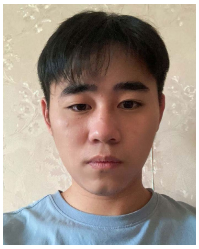

SIHAN LV is currently pursuing the master's degree with the National Key Laboratory of Science and Technology on Antennas and Microwaves, Xidian University. He has co-invented three Chinese patents. His main research interests include 5G millimeter wave terminal antennas and millimeter wave MIMO antenna technology.

LUYU ZHAO (Senior Member, IEEE) was born in Xi'an, China, in 1984. He received the B.Eng. degree from Xidian University, Xi'an, in 2007, and the Ph.D. degree from The Chinese University of Hong Kong, Sha Tin, Hong Kong, in 2014.

From 2007 to 2009, he was with the Key Laboratory of Antennas and Microwave Technology, Xidian University, as a Research Assistant, where he was involved in software and hardware implementation of RF identification (RFID) technologies. From 2014 to 2015, he was a Postdoctoral Fellow at The Chinese University of Hong Kong. From October 2015 to October 2016, he was with Wyzdom Wireless Company Ltd., where he was a Co-Founder and the CTO. He has been an Associate Professor with the National Key Laboratory of Antennas and Microwave Technology, Xidian University, since 2016. He has also been with Lambda Communication Company Ltd., since 2019. His current research interests include design and application of multiple antenna systems for next generation mobile communication systems, innovative passive RF and microwave components and systems, millimeter wave and terahertz antenna array, and meta-material-based or inspired antenna arrays.

Dr. Zhao was a recipient of the Best Student Paper Award of 2013 IEEE 14th HK AP/MTT Postgraduate Conference, the Honorable Mention Award of 2017 Asia-Pacific Conference on Antenna and Propagation, and the Best Paper Award of IEEE ICEICT 2019.

GUAN-LONG HUANG (Senior Member, IEEE) received the B.E. degree in electronic information engineering from Harbin Institute of Technology, Harbin, China, and the Ph.D. degree in electrical and computer engineering from the National University of Singapore, Singapore.

He is currently a Full Professor with Foshan University, Foshan, Guangdong, China. He is also a Joint-Researcher with Peng Cheng Laboratory, Shenzhen, Guangdong, China. Prior to join the current university, he has been with Shenzhen University as an Associate Professor, Nokia Solutions and Networks System Technology as a Senior Antenna Specialist, and the Temasek Laboratories, National University of Singapore, as a Research Scientist, from 2011 to 2020. He has authored or coauthored more than 100 papers in journals and conferences. His research interests include design and implementation of high-performance antenna arrays, 5G base-station and mobile RF front-end devices/antennas, lens antenna, phased antenna arrays, liquid metal antenna, and 3-D printing technology in microwave applications. He was a TPC member and special session organizer of several international conferences. He was a recipient of the Fok Ying-Tong Education Foundation Award from the Ministry of Education of the People's Republic of China, in 2020, the Best Reviewer Award of IEEE Antennas and Wireless Propagation Letters and IEEE Transactions on Antennas and Propagation from the IEEE Antenna and Propagation Society, in 2019 and 2020, respectively, and the Foundation for Distinguished Young Talents in Higher Education of Guangdong Province, China, in 2017.

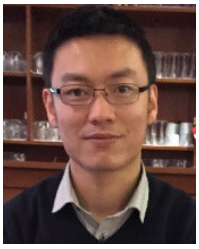

XIAOMING CHEN (Senior Member, IEEE) received the B.Sc. degree in electrical engineering from Northwestern Polytechnical University, Xi'an, China, in 2006, and the M.Sc. and Ph.D. degrees in electrical engineering from Chalmers University of Technology, Göthenburg, Sweden, in 2007 and 2012, respectively. From 2013 to 2014, he was a Postdoctoral Researcher at Chalmers University of Technology. From 2014 to 2017, he was with Qamcom Research and Technology AB, Göthenburg. Since 2017, he has been a Professor with Xi'an Jiaotong University, Xi'an. His research interests include MIMO antennas, over-the-air testing, reverberation chambers, and hardware impairments and mitigation. He received the IEEE Outstanding AE Awards, in 2018, 2019, and 2020, and the International Union of Radio Science (URSI) Young Scientist Award, in 2017. He serves as an Associate Editor for IEEE Antennas and Wireless Propagation Letters.

WEI LIN (Senior Member, IEEE) received the bachelor's and master's degrees in electronic engineering from South China University of Technology, Guangzhou, China, in 2009 and 2012, respectively, and the Ph.D. degree in electronic engineering from the City University of Hong Kong, Hong Kong, in 2016.

He worked as a Research Associate with Nanyang Technological University, Singapore, from August 2012 to August 2013, and a Postdoctoral Research Associate with The University of Technology Sydney, Ultimo, NSW, Australia, from October 2016 to September 2018, where he is currently a Chancellor's Postdoctoral Research Fellow with the Global Big Data Technologies Centre, Faculty of Engineering and IT, School of Electrical and Data Engineering. His research interests include the designs of circularly polarized antennas, electrically small antennas, reconfigurable antennas, HF antennas, satellite antennas, millimeter-wave antennas, wireless power transfer, terahertz devices, and their applications.

Dr. Lin has received many academic awards, which mainly include the Australia Research Council (ARC) Discovery Early Career Researcher Award (DECRA2021), the 2019 Raj Mittra Travel Grant (RMTG) from the IEEE AP-Society, the Best Paper Award (First Prize) at the International Symposium on Antennas and Propagation (ISAP 2018), the Best Young Professional Paper Award (First prize) at the 3rd Australian Microwave Symposium (AMS2018), the Best Poster Paper Award at the 2nd International Conference on Electromagnetic Materials and Technologies for the Future (EM-MTF2017), the Talent Development Scholarship from Hong Kong Government, and the Young Scientist Award at the IEEE Region 10 Conference (TENCON2015). He was a recipient of an Outstanding Reviewer Award from the IEEE Antennas and Wireless Propagation Letters, in 2018, and the IEEE Transactions on Antennas and Propagation, in 2020.